ELSEVIER

International Journal of Mass Spectrometry 204 (2001) 197–208

International Journal of Mass Spectrometry

Photodesorption of carbonyl from $Pt_3(CO)_n^-$ (n = 1–6)

Yang Shi, Vassil A. Spasov, Kent M. Ervin*

Department of Chemistry and Chemical Physics Program, University of Nevada, Reno, NV 89557, USA

Received 25 January 2000; accepted 13 May 2000

Abstract

The photodesorption of CO from $Pt_3(CO)_n^-$ (n = 1–6) has been studied in laser excitation experiments. Loss of CO is the major product channel for each species. The time-resolved profiles of photodesorption product ions are measured following excitation with visible laser radiation, 420–800 nm. Slow fragmentation on the 10 μs–1 ms time scale is observed for n = 2, 3, and 6. The binding energies of carbonyl in $Pt_3(CO)_n^-$ (n = 2, 3, 6) are derived by fitting these time profiles using a statistical unimolecular dissociation model. The recommended CO binding energies of $Pt_3(CO)_3^-$ and $Pt_3(CO)_6^-$ are 206 ± 14 and 166 ± 14 kJ/mol, respectively, in good agreement with previous results from threshold collision-induced dissociation measurements. For $Pt_3(CO)_2^-$, a minor second product channel Pt_2CO^- + PtCO is observed in addition to CO photodesorption. Experimental evidence suggests that there is more than one isomer for $Pt_3(CO)_2^-$ species. (Int J Mass Spectrom 204 (2001) 197–208) © 2001 Elsevier Science B.V.

Keywords: Photodissociation; Photodesorption; Platinum cluster carbonyls; Metal–ligand interactions

1. Introduction

The interactions between metal clusters and ligands or adsorbates are important as models in gas–surface catalytic processes [1–5] and the clusters themselves may act as catalysts [6]. Measurements of dissociation energies in metal–ligand systems are important also for providing benchmarks for theoretical calculations increasingly being applied to metal clusters and organometallics [7,8]. Energy-resolved threshold collision-induced dissociation or desorption (TCID) experiments have been dedicated to monometal carbonyl systems such as iron [9,10], vanadium [11], chromium [12], cobalt [13], and nickel [10], and multimetal carbonyl systems [14–16] including $Pt_m(CO)_n^-$ and $Pd_3(CO)_n^-$. The measurements reveal information about the structures and thermochemistry of these ligated metal clusters.

We have recently developed the capability to perform photodissociation or photodesorption (PD) lifetime measurements as an alternative approach to TCID [17,18]. Both experiments, TCID and PD, can be conducted using our guided ion beam tandem mass spectrometer [19]. The basic idea of the PD lifetime experiment is to measure the intensity of fragment ions as a function of time after laser excitation, from which the lifetimes of photoexcited clusters can be obtained. Statistical theories of unimolecular decomposition are used to model the lifetimes and extract the binding energies. The PD lifetime method avoids potential weaknesses in the analysis of TCID, e.g. the uncertainty of collisional energy transfer efficiency. Also, PD allows direct observation of the time-

* Corresponding author. E-mail: ervin@chem.unr.edu

1387-3806/01/$20.00 © 2001 Elsevier Science B.V. All rights reserved
PII S1387-3806(00)00364-X

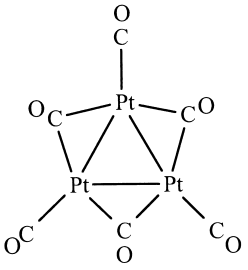

Fig. 1. Structure of $[Pt_3(CO)_6]^{2-}$ in solution as characterized by Chini and co-workers [23,24] and proposed structure of gas-phase $Pt_3(CO)_6^-$ [14,15].

dependent fragmentation, rather than a kinetic shift in TCID [20], simplifying the dissociation energy determination. Comparisons of TCID and PD have been made for pure metal cluster ions, Al_n^+ [21], Ag_n^- (n = 7–11) [17], Ag_n^+ (n = 8–21) [22], and Au_n^- (n = 6, 7) [18]. Our PD and TCID results on silver and gold cluster anions using the same cluster source [17,18] generally validate the procedures and assumptions used in TCID experiments and data analysis in spite of some small offsets.

This work extends PD measurements to adsorbate–metal cluster systems, namely $Pt_3(CO)_n^-$ (n = 1–6), for which TCID results were previously reported [14,15]. The binding energies of CO to Pt_3^- cluster obtained by TCID indicate two different types of binding sites, three terminal sites (100–180 kJ/mol) and three bridged sites (about 220 kJ/mol), in agreement with the structure [23,24] of $[Pt_3(\mu\text{-}CO)_3(CO)_3]^{2-}$ in solution as depicted in Fig. 1. In this work, the dissociation kinetics of photoexcited $Pt_3(CO)_n^-$ is investigated experimentally. The results are compared with our previous TCID experiments [14,15].

2. Experiments and data analysis

The guided ion beam tandem mass spectrometer used in this work and the procedures for the photodissociation experiment and data analysis have been presented in detail [17,19]. Briefly, platinum carbonyl cluster anions are produced using a flow tube reactor source. The buffer gas includes helium (90%) and argon (10%) at a total pressure of about 350 mTorr. Platinum cluster anions are produced at a platinum metal cathode held at about −1.5 kV in a dc discharge sputtering source. Carbon monoxide is introduced downstream of the discharge region. After extraction from the flow tube and acceleration, the cluster ions of interest are mass selected by a magnetic sector and are then injected into an octopole ion beam guide at a fixed translational energy (~3 eV). An excimer-pumped dye laser system (Lambda Physik LPX140i/LPD 3001) is used to generate tunable laser light (420–800 nm) for photodesorption experiments. The dye laser beam is collimated and directed coaxially along the center of the octopole to overlap with the cluster ion beam. The mass-selected cluster ions absorb photons upon irradiation and subsequently dissociate. Fragment ions are collected with high efficiency by the octopole and are then detected by a quadrupole mass spectrometer as a function of time from the laser pulse. Ions that are near the detector end of the octopole at the time of the laser pulse arrive at the detector first, followed at later times by those nearer the source end of the octopole. Thus, the spatial distribution of the ions is converted into a product time distribution. The ion time-of-arrival spectrum is accumulated with a multichannel scaler (EG&G Turbo-MCS) for up to 10^5 laser shots to obtain an adequate signal-to-noise ratio. The product ion intensity shows a rising time profile if the dissociation lifetime matches the experimental time window. High photon energies lead to prompt desorption and a rectangular product time profile when proper alignment between the ion and laser beam is achieved.

To extract the dissociation energies from experimental time profiles, Rice-Ramsperger-Kassel-Marcus (RRKM) rate theory for unimolecular dissociation is applied to model the experimental photodesorption lifetimes [21,25]. The RRKM microcanonical rate constant $k(E, J)$ for dissociation at a total internal energy E and angular momentum J is

$$k(E, J) = \sigma \frac{W^{\ddagger}(E - E_0, J)}{h\rho(E, J)} \quad (1)$$

where $W^{\ddagger}(E - E_0, J)$ is the number of states at the transition state, $\rho(E, J)$ is the density of states of the

energized cluster, E_0 is the dissociation activation energy at 0 K, and σ is the reaction path degeneracy. The dependence of product yield on time after the laser pulse is convoluted over the internal energy and rotational angular momentum distributions of the cluster ions. The product intensity versus time is formulated as

$$I(t) = C \int_0^\infty \int_0^\infty P(E_i, J) \cdot [1 - e^{-k(E_i+E_{h\nu}, J)(t-t_0)}]\, dJ\, dE_i \quad (2)$$

where C is a scaling constant, $P(E_i, J)$ is the Boltzmann rovibrational energy and angular momentum distribution of the cluster ions at 300 K, $E_{h\nu}$ is the laser excitation energy, and t_0 is the instrumental delay time. A modified version of the CRUNCH program [26] is used to calculate the internal energy distribution and to convolute and fit the experimental time profile to extract the desorption threshold energies.

For photodissociation experiments, E_0 is equal to the thermochemical dissociation energy if there is no reverse activation barrier. In the dissociation of cluster ions, potential energy barriers in excess of the reaction endothermicities are not usually expected because of the strong long-range attractive potential between the dissociation products [27]. Loss of CO is a heterolytic dissociation process, which on theoretical grounds [28] should have no dissociation barrier. Further, earlier kinetics measurements of the fast reverse association rates of Pt_3^- with CO indicate that any barrier on the path of desorption of carbonyl from Pt_3^- is less than 4.5 kJ/mol [29,30]. Therefore, the derived E_0 will be directly equated with the CO binding energy in the present experiment.

The experimental time profiles are modeled using tight and loose transition states (TS) as limiting cases [16,17,20]. The tight-limit TS model treats the TS as identical to the reactant cluster, except with one vibrational mode removed as the reaction coordinate. This model represents the tightest reasonable transition state, and gives lower limits for the RRKM rates and derived dissociation energies. In the loose-limit TS model ("phase space limit" [20]), the TS is positioned variationally at the top of the centrifugal dissociation barrier for the ion–induced-dipole potential, and vibrational and rotational parameters are identical to those of the free fragments. This model represents an upper limit for RRKM rates and dissociation energies, and is most appropriate for the barrierless CO desorption processes. The vibrational and rotational parameters for the RRKM calculations are identical to those used by Grushow and Ervin [15] for TCID of platinum carbonyl cluster anions.

The uncertainties of the reported binding energies are composed of errors from several sources, including the uncertainty of vibrational frequencies, the reproducibility of independent data sets, and statistical uncertainties of the nonlinear least-squares fits for individual time profiles. For vibrational frequencies, the fits are repeated with all the frequencies increased or decreased by 50% from their original values. The resulting limiting values of the binding energy typically differ by 5–10 kJ/mol. The reproducibility test includes two kinds of experiments: (1) time profiles obtained using different laser excitation photon energies while other conditions are the same and (2) time profiles acquired at different experimental sessions with variations of other experimental conditions. The total uncertainty is the root-sum-of-squares of the individual error estimates. The final uncertainty represents an estimate of $\pm 2\sigma$, but does not include possible systematic errors in the analysis models.

3. Results

3.1. General features

Upon photoexcitation, all $Pt_3(CO)_n^-$ (n = 1–6) ions undergo photodesorption by loss of a single CO. Other fragmentation channels are minor for n = 2 with loss of PtCO and nonexistent for other species. Three species, $Pt_3(CO)_2^-$, $Pt_3(CO)_3^-$, and $Pt_3(CO)_6^-$, show slow-rising product ion time profiles in the available wavelength range. For the three other clusters, only fast dissociation with rectangular product time profiles (lifetimes shorter than 10 μs) are observed within the available dye laser range (420–800

nm). For $Pt_3(CO)_4^-$ and $Pt_3(CO)_5^-$, TCID results [15] indicate that their CO binding energies are too small for the lifetime measurement even at the longest wavelengths available with our laser system. TCID experiments [15] indicate that $Pt_3(CO)^-$ has a binding energy comparable with the applied photon energy range, and our RRKM model predicts that a slow process should be observed in the available photon energy range. One possible explanation for the lack of a slow process might be that a five-atom system is too small to show a statistical fragmentation. The possibility of a two photon absorption dominating can not be excluded, but it is unlikely for the laser power density used. In previous photodissociation experiments of metal clusters including Al_n^+ [21], Ag_n^- [17], Ag_n^+ [31], and Au_n^- [18], only clusters of more than five atoms showed a statistical dissociation process on the 10–1000 μs scale.

Laser power dependence measurements are performed at the wavelengths where the slow dissociation is observed. The measurements indicate that the desorption is a single photon process for reactants $Pt_3(CO)_2^-$ at 450–480 nm, $Pt_3(CO)_3^-$ at 620–670 nm, and $Pt_3(CO)_6^-$ at 670–730 nm. The power dependences for the reactions $Pt_3(CO)_2^- + h\nu \rightarrow Pt_3(CO)^- + CO$, $Pt_3(CO)_3^- + h\nu \rightarrow Pt_3(CO)_2^- + CO$, and $Pt_3(CO)_6^- + h\nu \rightarrow Pt_3(CO)_5^- + CO$ at fixed wavelengths are shown in Fig. 2. The unit slopes on a logarithmic scale are consistent with single photon absorption. Power dependence measurements can be misleading in the case of saturated transitions, but only single-photon absorptions are consistent with the bond energy results and previous TCID measurements. No attempt was made to measure photodissociation threshold energies. Besides experimental difficulties in normalizing spectra measured in different laser dye wavelength regions, threshold experiments would be subject to kinetic shifts, competitive radiative emission, and multiphoton effects.

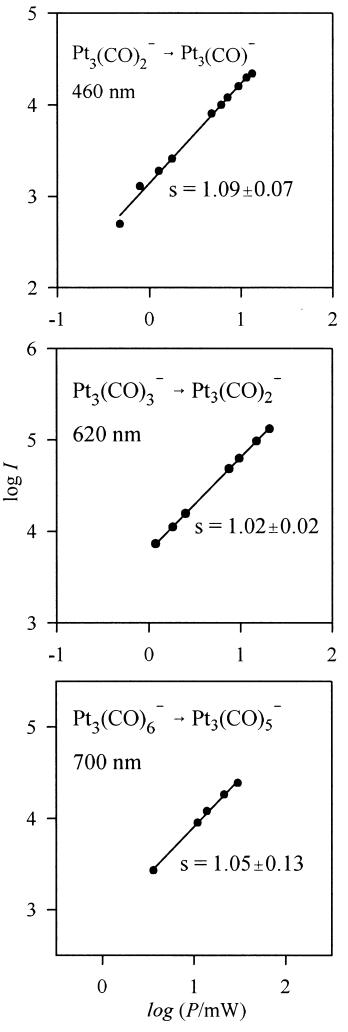

Fig. 2. Power dependence measurement for $Pt_3(CO)_2^- \rightarrow Pt_3(CO) + CO$ at 460 nm, $Pt_3(CO)_3^- \rightarrow Pt_3(CO)_2^- + CO$ at 620 nm, and $Pt_3(CO)_6^- \rightarrow Pt_3(CO)_5^- + CO$ at 700 nm. The indicated values of the slopes are obtained by linear regression.

3.2. Possible competitive processes

For anionic clusters with similar electron affinities and dissociation energies, electron photodetachment and fragmentation processes can be competitive in the photoexcited clusters. This competition has been observed in silver anions [17,32]. There might also be other competitive processes such as radiative emission, thermal electron emission, and other dissociative channels [33–38]. To extract the desired binding energy from a lifetime measurement, the importance of such competitive processes must be assessed. For $Pt_3(CO)_n^-$ species, the predominant dissociative channel is loss of CO. To address the possibility of

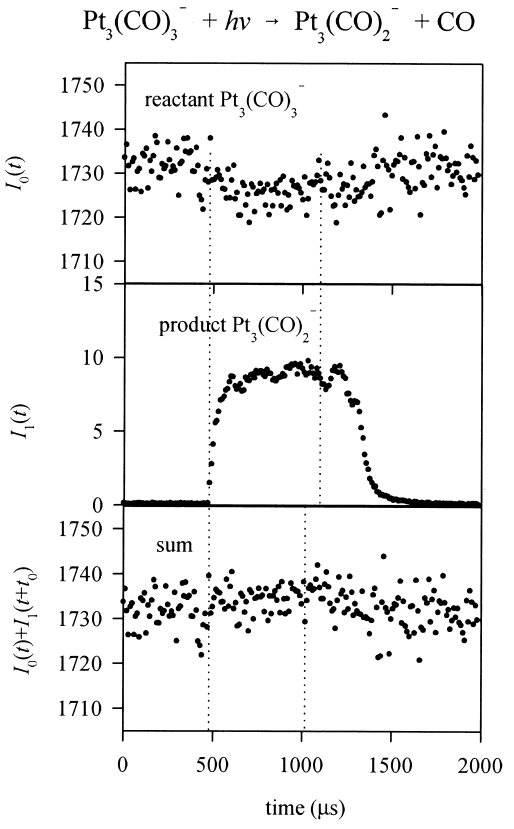

Fig. 3. Time profiles of reactant depletion, product appearance, and the sum of reactants and products for $Pt_3(CO)_3^-$ at 620 nm. The sum is obtained with $I_{tot}(t) = I_0(t) + I_1(t + t_0)$, where t_0 accounts for the time products spend in the quadrupole mass spectrometer. The vertical dotted lines delimit the ions inside the octopole at the time of the laser pulse.

electron loss, product appearance and reactant depletion measurements are performed [17]. As a representative example, the product and reactant depletion profiles of $Pt_3(CO)_3^-$ at 620 nm are shown in Fig. 3. The depletion of reactant is only 0.5% of the total intensity when the dye laser output is 110 μJ/pulse. Compared with silver cluster anions [17], the depletion observed here is much smaller. The observed product formation accounts for all of the reactant depletion. In other words, there is no competitive direct or statistical electron emission process, nor other dissociation process in photoexcited $Pt_3(CO)_3^-$. Ganteför and co-workers have measured the photoelectron spectra (PES) of $Pt_3(CO)_n^-$ ($n = 0$–6) [39,40]. The electron emission signal just emerges at an electron binding energy of 220 kJ/mol for photoexcited $Pt_3(CO)_3^-$ [39,40]. The photon excitation energy for 620 nm is 193 kJ/mol and the average initial thermal energy is 29 kJ/mol, for a total mean internal energy of 222 kJ/mol. Therefore, the electron emission process can not compete with the carbonyl desorption process at 620 nm. For $Pt_3(CO)_2^-$ and $Pt_3(CO)_6^-$, the product appearance and reactant depletion measurements also show negligible electron loss processes in the experimental energy range. Hence, electron emission is not an important decay channel in these photoexcited platinum carbonyl clusters.

Another possible competing decay process in photoexcited platinum carbonyl clusters is radiative relaxation. Since prompt fluorescence involves a different precursor than statistical decomposition, it need not be considered as a competing process for the dissociation energy extraction [17]. On the other hand, slow radiative relaxation from an energy-randomized intermediate might be competitive. Blackbody radiation from pure metal clusters has been observed experimentally [33,35]. For platinum carbonyl cluster anions, there are vibrational modes with high frequencies and the carbonyl has a small dipole moment, which could make the radiative emission process faster than for the pure metal clusters [41]. In the worst case, the absorption of a photon at 460 nm will give $Pt_3(CO)_2^-$ internal energy equal to a temperature of 2300 K, resulting in substantial population of vibrationally excited states. Hence, infrared radiative emission could in principle be an important process for photoexcited clusters. Infrared radiative relaxation has been investigated for many gas phase ions, as reviewed by Dunbar [41]. The measured lifetimes for radiative emission are greater than 1 ms for most ions, but a few have lifetimes in the range of hundreds of microseconds, which would be competitive with our observed desorption processes. Radiative cooling rates of V_{13}^+ were measured recently; at an internal temperature of 2000 K, the radiative lifetime is about 200 μs [42]. Experimentally, our appearance–depletion measurement is totally blind to the radiative emission process. Radiative emission will therefore

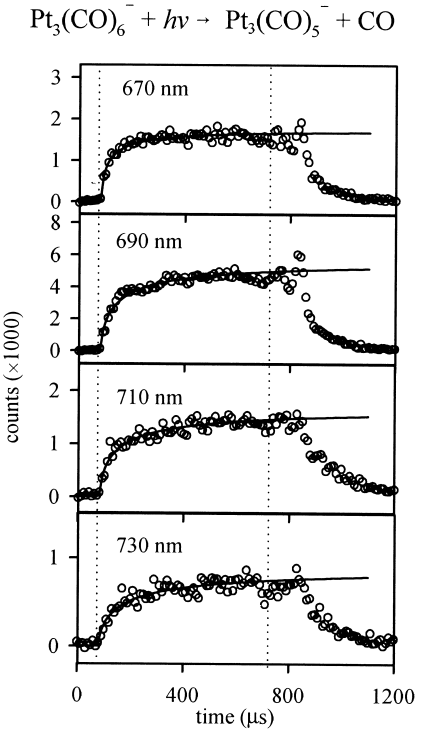

Fig. 4. Product appearance time profiles (points) measured at several photon energies for $Pt_3(CO)_6^- \rightarrow Pt_3(CO)_5^- + CO$ with fits (lines) of Eq. (2). The vertical dotted lines delimit the ions inside the octopole at the time of the laser pulse.

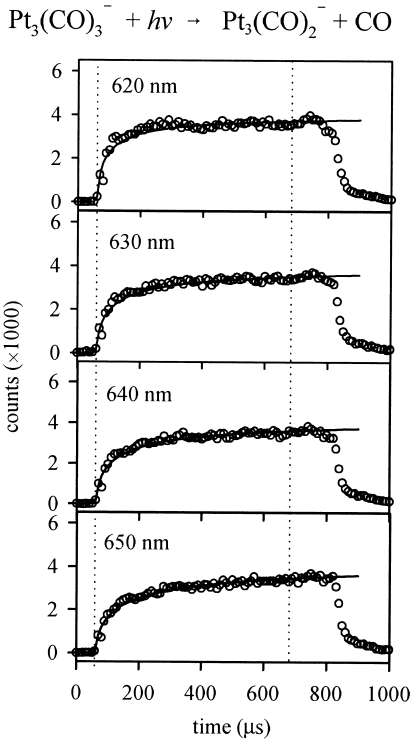

Fig. 5. Product appearance time profiles (points) measured at several photon energies for $Pt_3(CO)_3^- \rightarrow Pt_3(CO)_2^- + CO$ with fits (lines) of Eq. (2). The vertical dotted lines delimit the ions inside the octopole at the time of the laser pulse.

be neglected in this work. If the radiative relaxation process is significant here, this neglect will make the derived binding energies lower than the true values.

The overall kinetic scheme can be summarized as photoexcitation of $Pt_3(CO)_n^-$,

$$Pt_3(CO)_n^- + h\nu \rightarrow [Pt_3(CO)_n^-]^* \quad (3)$$

to form the long-lived intermediate $[Pt_3(CO)_n^-]^*$, followed by statistical decomposition,

$$[Pt_3(CO)_n^-]^* \rightarrow Pt_3(CO)_{n-1}^- + CO \quad (4)$$

The experimental time profiles of product ion appearance are fit directly using Eq. (2) without further correction. Typical data sets for $Pt_3(CO)_n^-$ at various wavelengths are shown in Figs. 4–6 for $n = 6$, 3, and 2. The fits of Eq. (2) are shown in Figs. 4–6, and the average E_0 values from all data sets are given in Table 1.

3.3. Photodesorption of $Pt_3(CO)_6^-$ and $Pt_3(CO)_3^-$

The slow-rising time profiles of the sole product, $Pt_3(CO)_5^-$, from $Pt_3(CO)_6^-$ can be observed when the laser wavelength is longer than 670 nm. The time profiles, Fig. 4, are measured at 670–730 nm (164–179 kJ/mol photoexcitation plus a mean initial internal energy of 48 kJ/mol). As shown in Table 1, the averages for all time profiles at different wavelengths indicate that there is no systematic wavelength dependence of the extracted CO binding energy using the loose TS model, but there is a minor but apparent wavelength dependence for the tight TS model values. For the tight TS, the extracted energy decreases with increasing laser wavelength. Self-consistency implies that the loose TS model is more valid. The recommended CO binding energy of $Pt_3(CO)_6^-$ is 166 ± 14 kJ/mol using the loose TS model.

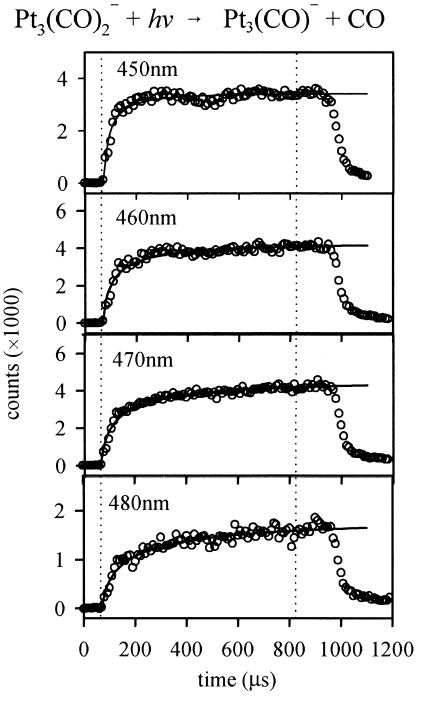

Fig. 6. Product appearance time profiles (points) measured at several photon energies for $Pt_3(CO)_2^- \rightarrow Pt_3(CO)^- + CO$ with fits (lines) of Eq. (2). The vertical dotted lines delimit the ions inside the octopole at the time of the laser pulse.

The photodesorption of $Pt_3(CO)_3^-$ shows only one product channel, the loss of a single CO to yield $Pt_3(CO)_2^-$. Slow-rising time profiles of the product ions are observed at excitation laser wavelengths of 620–650 nm (184–193 kJ/mol photoexcitation plus a mean internal energy of 29 kJ/mol), as shown in Fig. 5. As shown in Table 1, the tight TS model values exhibits an apparent wavelength dependence, for which the CO binding energy decreases with an increase of photon wavelength. The E_0 values from the loose TS model are well within statistical fluctuations. The CO binding energy for $Pt_3(CO)_3^-$ is 206 ± 14 kJ/mol using the loose TS model.

3.4. Photodesorption of $Pt_3(CO)_2^-$

Photodissociation of $Pt_3(CO)_2^-$ using 450–480 nm photons (249–266 kJ/mol photoexcitation plus 22 kJ/mol initial mean internal energy) exhibits predominately the carbonyl loss channel, with the intensity of product $Pt_3(CO)^-$ a hundred times stronger than that of $Pt_2(CO)^-$. In TCID of $Pt_3(CO)_2^-$ [14,15], in contrast, two product channels with comparable intensities, $Pt_3(CO)^- + CO$ and $Pt_2(CO)^- + PtCO$, are observed [14,15]. The TCID experiments [14,15] also show that the cross sections of these two channels cross each other, with loss of CO as the predominant channel when the collision energy in the center-of-mass frame ($E_{c.m.}$) is less than 2.3 eV and loss of PtCO as the main channel at higher energies. The lowest photoactivation energy used in the PD experiment, 2.81 eV at 480 nm including the mean initial internal energy, is well above the crossing point in the TCID. It is interesting to find reversed product ratios for the TCID and PD experiments since it should not matter how the energy is introduced if the products are from the same intermediate and the dissociation is statistical. We repeated the TCID and PD experiments under identical source and detection conditions and found the same results, excluding the possibility of detection discrimination or different ion distributions.

It can be seen in Table 1 that the CO binding

Table 1
E_0 (kJ/mol) for $Pt_3(CO)_n^- \rightarrow Pt_3(CO)_{n-1}^- + CO$ at various wavelengths[a]

n	λ (nm)	Loose TS	Intermed. TS	Tight TS
2	450	273.3 ± 4.9	269.9 ± 3.6	233.6 ± 2.4
	460	275.4 ± 3.9	269.6 ± 3.6	232.4 ± 1.6
	470	276.5 ± 4.0	270.5 ± 3.7	230.7 ± 1.4
	480	277.3 ± 6.0	270.8 ± 4.6	228.6 ± 1.5
3	620	207.5 ± 3.5		166.0 ± 1.5
	630	207.7 ± 3.1		165.2 ± 1.4
	640	206.5 ± 3.7		163.7 ± 1.4
	650	205.9 ± 4.1		162.0 ± 1.3
6	670	165.9 ± 3.1		127.8 ± 2.0
	680	166.2 ± 1.4		126.2 ± 3.6
	690	165.8 ± 3.9		125.6 ± 4.1
	700	165.6 ± 4.0		124.9 ± 3.6
	710	165.6 ± 2.8		125.1 ± 2.5
	720	166.3 ± 3.7		125.0 ± 3.0
	730	165.2 ± 4.1		124.7 ± 1.2

[a] The error bars represent ±1 estimated standard deviation for several experiments at each wavelength, and do not include the uncertainty of vibrational frequencies.

energies for $Pt_3(CO)_2^-$ from the RRKM model show apparent wavelength dependences for both the tight and loose TS models, in opposite directions. This systematic photon wavelength dependence indicates that neither TS model reproduces the observed photon energy dependence of unimolecular dissociation and that the process of CO desorption from $Pt_3(CO)_2^-$ should be described by an intermediate transition state model [16,17,43,44]. The intermediate TS model employs a tight, fixed transition state with frequencies identical to the parent cluster except for removal of one mode for the reaction coordinate, and the reduction of four transition mode frequencies for CO loss. The fits using the four frequencies divided by two as typically used [17,21] still show a small wavelength dependence. Reducing the frequencies to 5% of their original values yields binding energies free of apparent wavelength dependence [45]. The E_0 values from fits using this TS model are also shown in Table 1. The recommended CO binding energy in $Pt_3(CO)_2^-$ is 270 ± 13 kJ/mol using the intermediate TS model compared with 275 ± 18 kJ/mol from the loose TS model and 220 ± 50 kJ/mol from TCID.

There are some unique features in TCID and PD of $Pt_3(CO)_2^-$. First, the PD result just barely agrees with the TCID value within the error bars, and the direction of the deviation is opposite to the expectation that the TCID value is an upper limit (vide infra). Second, PD and TCID show reversed product ratios at the same total energy. Finally, the cross sections of the two product channels cross in TCID. The TCID value for $Pt_3(CO)_2^-$ was originally derived without taking into account the possible competitive shift [14,15] due to the two product channels. Because of the existence of the second channel, a large uncertainty (±50 kJ/mol) was reported for $D(Pt_3CO^-–CO)$ in the TCID work. The neglected Pt_2CO^- channel is predominant over a wide energy range. To account for the competitive shift, we have attempted to use the recently developed competitive dissociation model [46,47] for simultaneously fitting the two product channels of TCID of $Pt_3(CO)_2^-$. Since the two channels involve different kinds of reactions, desorption of carbonyl and breakage of the metal skeleton, different TS models are required for these two processes. The loss of CO needs the loose TS model while the breakage of the metal cluster core requires the tight TS model [16,17]. The two TS models have different dependences of microcanonical rate constants $k(E, J)$ on internal energy and the two channels have different threshold energies, which could in principle cause the anomalous crossing. We applied transition state models including the combinations of loose–loose, tight–loose, tight–tight, and loose–tight for the two channels. None of these models yields reasonable fits for both channels, suggesting that the two channels might not be from the same reactant. Specifically, there might be more than one isomer for reactant $Pt_3(CO)_2^-$. The presence of isomers of $Pt_3(CO)_2^-$ could also explain the different product patterns of TCID and PD experiments, say if one isomer is transparent to photoexcitation whereas another isomer absorbs a photon and dissociates to form product $Pt_3(CO)^-$. Collisional excitation is effective for all isomers and would lead to both dissociation channels in TCID.

To ascertain the existence of isomers in $Pt_3(CO)_2^-$, we further investigated the effect of source conditions on TCID behavior. More extreme variation of source conditions is used than was done in previous work [15]. In Fig. 7, two source conditions are compared, both with the argon buffer gas flow fixed at 0.45 STP (standard temperature and pressure) L/min but with the helium gas flow changed to (a) 6.5 STP L/min and (b) 1.5 STP L/min. The total flow tube pressures are (a) 0.34 Torr and (b) 0.14 Torr, respectively. It can be seen that channel Pt_2CO^- + PtCO remains almost the same while channel Pt_3CO^- + CO changes obviously to a higher threshold energy under condition (b). Competitive dissociation models with all four transition state model combinations are tried to fit the cross sections under condition (b) but still do not give satisfactory fits to both channels simultaneously. Fitting to the CO loss channel without considering competitive shift yields $D(Pt_3(CO)^-–CO)$ = 256 ± 46 kJ/mol using the loose TS model. This value still agrees with the original TCID result of 220 ± 50 kJ/mol within the large error bars, but is closer to PD result. If the extent of cluster ion thermalization were the only difference between the two measurements, there would be a higher temperature and more internal

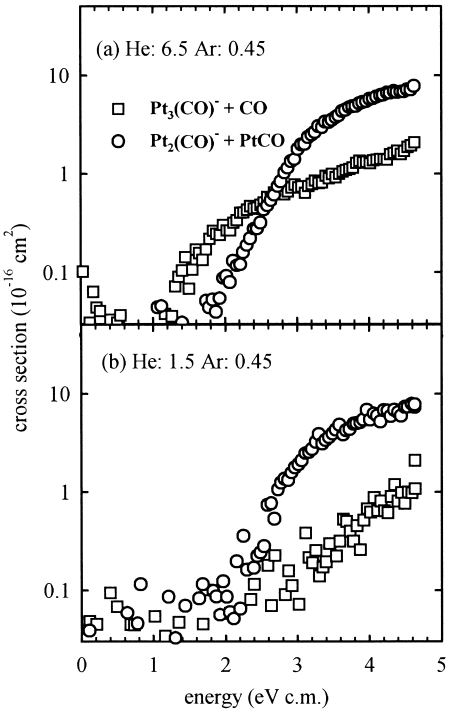

Fig. 7. TCID cross sections for reactions $Pt_3(CO)_2^- + Xe \rightarrow Pt_3(CO)^- + CO + Xe$ and $Pt_3(CO)_2^- + Xe \rightarrow Pt_2(CO)^- + PtCO + Xe$ at different gas flows in the flow tube reactor source: (a) He, 6.5 STP L/min; Ar, 0.45 STP L/min; p = 340 mTorr and (b) He, 1.5 STP L/min; Ar, 0.45 STP L/min; p = 140 mTorr. Circles represent channel $Pt_2(CO)^- + PtCO$ and squares represent $Pt_3(CO)^- + CO$.

energy in $Pt_3(CO)_2^-$ for the low-pressure condition (b), which would cause the apparent cross section thresholds to shift to lower collisional energy. In contradiction, the experimental TCID cross section behaves in an opposite way. Hence, it is not just a question of thermalization, but rather the different source conditions yield different isomer compositions, causing different behaviors of the TCID cross section. Perhaps the higher pressure for condition (a) allows a high energy isomer to be trapped in a metastable well through stabilizing collisions. Unfortunately, PD lifetimes could not be measured for condition (b) because of low ion intensities. Comparison of the TCID cross sections of $Pt_3(CO)_n^-$ (n = 1–6) series [15] at condition (a) also finds $Pt_3(CO)_2^-$ is unique. The absolute cross section of reaction

Table 2
Carbonyl binding energies, $D_0[Pt_3(CO)_{n-1}^- – CO]$, in kJ/mol

n	TCID[a]	PD[b]
1	220 ± 30	
2	220 ± 50	270 ± 13
3	220 ± 22	206 ± 14
4	103 ± 14	
5	110 ± 19	
6	180 ± 30	166 ± 14

[a] Threshold collision-induced dissociation, see [15].
[b] Photodissociation kinetics, this work.

$Pt_3(CO)_2^- + Xe \rightarrow Pt_3(CO)^- + CO + Xe$ is about one order magnitude smaller than for other values of n; there is no reason for this exception if all generated $Pt_3(CO)_n^-$ (n = 1–6) species follow the same molecular model. In comparison, the TCID cross sections of reactions $Pd_3(CO)_n^- + Xe \rightarrow Pd_3(CO)_{n-1}^- + CO + Xe$ (n = 1–6) monotonously increase with n [48], implying an uniform structure model is obeyed. In summary, the existence of isomers would be a reasonable explanation for all these unusual behaviors, namely, the crossing of the TCID cross sections, the different product ratios from TCID and PD, the disagreement of the threshold energies from TCID and PD, and the exceptionally small apparent cross section for TCID of $Pt_3(CO)_2^-$.

4. Discussion

The TCID and PD results for the CO binding energies of $Pt_3(CO)_n^-$ (n = 1–6) are summarized in Table 2 and Fig. 8. For $Pt_3(CO)_3^-$ and $Pt_3(CO)_6^-$, TCID yields slightly higher binding energies than does PD for both the tight and loose TS models. For the loose TS model, the results from the two experimental methods are fairly consistent and have overlapping error bars. As discussed previously [17], the TCID dissociation energies are strictly upper limits because the collisional energy transfer in the activation process could be less efficient than assumed by the threshold law used in the modeling. Although the electron loss process is not found in the PD experiments, it is not clear whether the radiative relaxation process is active. If the radiative relaxation process is

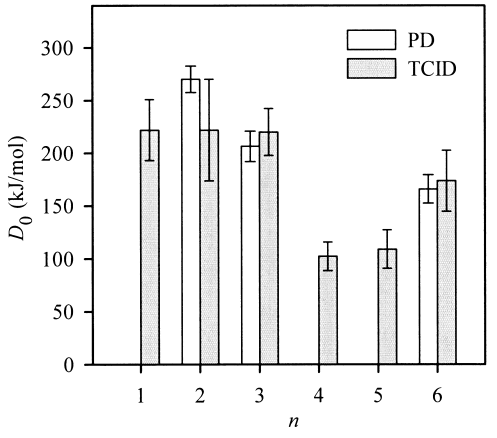

Fig. 8. Comparison of the recommended CO-loss desorption energies of $Pt_3(CO)_n^-$ measured by threshold collision-induced dissociation (TCID) from [15] (n = 1–6) and by photodesorption (PD) methods (n = 2, 3, 6) in this work.

significant in both TCID and PD experiments, then the extracted dissociation energies from TCID would be higher and the binding energies from PD will be lower than the true values, which would also contribute to the discrepancy between the TCID and PD results. The observed deviations between the two experimental methods are in the direction predicted for these possible effects. Nevertheless, the relatively small magnitudes of the deviations imply that the assumptions made in the two methods are reasonable. The effect of the choice of transition state model in the analysis is actually more critical than possible radiative emission or inefficient collisional activation.

The apparent dependence of derived CO binding energies on laser wavelength suggests that the loose TS model is more appropriate for the CO desorption processes from $Pt_3(CO)_3^-$ and $Pt_3(CO)_6^-$ than is the tight TS model. That is consistent with the previous treatment [15,28], but this evidence is not definitive because of experimental uncertainties and the limited practical wavelength range over which the dissociation lifetime can be measured. A loose transition state is most appropriate for ionic clusters with no barrier to dissociation in excess of the endothermicity and the rupture of a single localized bond [20]. The CO binding energies from the TCID and PD experiments using the loose TS model also agree with each other better than do the values of the tight TS model. Hence, the values from the loose TS model are recommended. The values from the tight TS model serve as lower limits.

For $Pt_3(CO)_2^-$, the comparison of PD and TCID under different source conditions points to the existence of at least two $Pt_3(CO)_2^-$ isomers. However, it is difficult to identify the number of isomers or their structures and stability. The CO dissociation energy from the TCID and PD experiments have overlapping error bars, but it is improper to compare the two experiments because different isomers might be probed. The PD experiment is effective only for those isomers with high photon absorption cross section, while TCID works for all kinds of isomers although the energy transfer efficiencies might be slightly different for each isomer. To repeat the TCID and PD experiments on $Pt_3(CO)_2^-$ with a different cluster source, especially one with annealing, would be helpful.

Grushow and Ervin [15] interpreted the TCID results as showing that the bridging carbonyls have higher binding energies than the terminal carbonyls in $Pt_3(CO)_n^-$, where n = 1–3 are bridging with higher binding energy and n = 4–6 are terminally bound with lower binding energy. The PD results are consistent with this interpretation and the model shown in Fig. 1. However, the slightly higher binding energy for n = 2 could indicate a more complicated sequence of structures than originally envisioned in the stepwise addition processes.

Theoretical calculations give ambiguous comparisons. Balasubramanian and co-worker [49] showed that terminal bonding between Pt_2 and CO leads to a less stable equilibrium complex than the bridge bonding, D = 205 kJ/mol for bridged versus D = 110 kJ/mol for terminal. That agrees with our assignments of bridging and terminal binding sites. Recent density functional theory calculations by Grönbeck and Andreoni [50] on neutral Pt_3CO, however, indicate that the terminal and edge-bridged sites have similar binding energy for CO, 260 and 240 kJ/mol, respectively. This result suggests that highly uncoordinated species have large CO binding energies regardless of the binding site. That is still consistent with the

experimental result that the binding energy drops sharply once the three bridged positions are completely filled. The possible existence of a three-fold face-bridging carbonyl, as proposed in the study of $Pd_3(CO)_n^-$ [48], can not be eliminated experimentally but it seems unfavorable on the basis of calculations [50–52] and surface studies [53,54]. High-level theoretical calculations on the anionic triplatinum carbonyls would be helpful to resolve these questions. Any theoretical treatment needs to be able to reproduce the binding energies for the whole set, $n = 1$–6 in Fig. 8, to give confidence in predicted structures for stepwise addition of the carbonyls.

5. Conclusion

The desorption kinetics of photoactived triplatinum carbonyl cluster anions, $Pt_3(CO)_n^-$ ($n = 2$, 3, 6), has been studied in photodissociation lifetime experiments. Only one desorption channel, loss of CO, is observed for species $n = 3$ and 6. No prompt or delayed electron loss is observed for these clusters. The CO binding energies obtained from the PD experiments are in good agreement with previous TCID results, which validates the application of the TCID method in adsorbate–metal cluster systems. These experiments also suggest that the loose TS model is more appropriate than the tight TS model for the platinum carbonyl clusters. The PD and TCID results of $Pt_3(CO)_2^-$ also agree within each other's error bars, but unusual behavior is observed. The experiments suggest that there is more than one isomer of $Pt_3(CO)_2^-$ formed under current source conditions. High-level theoretical study is indispensable to clarify the remaining question about the isomers of $Pt_3(CO)_2^-$ and to verify the structural assignments of other $Pt_3(CO)_n^-$ species.

Acknowledgement

This research was supported by the National Science Foundation, grant no. CHE-9816206.

References

[1] D.C. Parent, S.L. Anderson, Chem. Rev. 92 (1992) 1541.
[2] P.B. Armentrout, in Metal–Ligand Interactions—Structure and Reactivity, N. Russo, D.R. Salahub (Eds.), Kluwer, Dordrecht, 1996, p. 23.
[3] D.M. Cox, A. Kaldor, P. Fayet, W. Eberhardt, R. Brickman, R. Sherwood, Z. Fu, D. Sondericher, in Novel Materials in Heterogeneous Catalysis, R.T.K. Baker, L.L. Murrell (Eds.), ACS, Washington, DC, 1990, p. 172.
[4] S.J. Riley, in Clusters of Atoms and Molecules II, H. Haberland (Ed.), Springer, Berlin, 1994, p. 221.
[5] J. Tsuji, Palladium Reagents and Catalysis, Wiley, New York, 1995.
[6] Y. Shi, K.M. Ervin, J. Chem. Phys. 108 (1998) 1757.
[7] T. Ziegler, in Density-Functional Methods in Chemistry and Material Science, M. Springborg (Ed.), Wiley, Chichester, 1997, p. 69.
[8] W. Ekardt, Metal Clusters, Wiley, Chichester, 1999.
[9] R.H. Schultz, K.C. Crellin, P.B. Armentrout, J. Am. Chem. Soc. 113 (1991) 8590.
[10] L.S. Sunderlin, D. Wang, R.R. Squires, J. Am. Chem. Soc. 114 (1992) 2788.
[11] M.R. Sievers, P.B. Armentrout, J. Phys. Chem. 99 (1995) 8135.
[12] F.A. Khan, D.E. Clemmer, R.H. Schultz, P.B. Armentrout, J. Phys. Chem. 97 (1993) 7978.
[13] S. Goebel, C.L. Haynes, F. Khan, P.B. Armentrout, J. Am. Chem. Soc. 117 (1995) 6994.
[14] A. Grushow, K.M. Ervin, J. Am. Chem. Soc. 117 (1995) 11612.
[15] A. Grushow, K.M. Ervin, J. Chem. Phys. 106 (1997) 9580.
[16] V.A. Spasov, T.-H. Lee, J.P. Maberry, K.M. Ervin, J. Chem. Phys. 110 (1999) 5208.
[17] Y. Shi, V.A. Spasov, K.M. Ervin, J. Chem. Phys. 111 (1999) 938.
[18] V.A. Spasov, Y. Shi, K.M. Ervin, Chem. Phys., submitted.
[19] V.F. DeTuri, P.A. Hintz, K.M. Ervin, J. Phys. Chem. A 101 (1997) 5969.
[20] M.T. Rodgers, K.M. Ervin, P.B. Armentrout, J. Chem. Phys. 106 (1997) 4499.
[21] U. Ray, M.F. Jarrold, J.E. Bower, J.S. Kraus, J. Chem. Phys. 91 (1989) 2912.
[22] U. Hild, G. Dietrich, S. Krückeberg, M. Lindinger, K. Lückenkirchen, L. Schweikhard, C. Walther, J. Ziegler, Phys. Rev. A 57 (1998) 2786.
[23] J.C. Calabrese, L.F. Dahl, A. Cavalieri, P. Chini, G. Longoni, S. Martinengo, J. Am. Chem. Soc. 96 (1974) 2616.
[24] G. Longoni, P. Chini, J. Am. Chem. Soc. 98 (1976) 7225.
[25] R.G. Gilbert, S.C. Smith, Theory of Unimolecular and Recombination Reactions, Blackwell Scientific, Boston, 1990.
[26] P.B. Armentrout, K.M. Ervin, CRUNCH, FORTRAN program, 1999.
[27] P.B. Armentrout, in Advances in Gas Phase Ion Chemistry, N.G. Adams, L.M. Babcock (Eds.), JAI Press, Greenwich, CT, 1992, p. 83.

[28] P.B. Armentrout, J. Simons, J. Am. Chem. Soc. 114 (1992) 8627.
[29] X. Ren, P.A. Hintz, K.M. Ervin, J. Chem. Phys. 99 (1993) 3575.
[30] P.A. Hintz, K.M. Ervin, J. Chem. Phys. 100 (1994) 5715.
[31] U. Hild, G. Dietrich, S. Krükeberg, M. Lindinger, K. Lükenkirchen, L. Schweikhard, C. Walther, J. Ziegler, Phys. Rev. A 57 (1998) 2786.
[32] L.-S. Zheng, C.M. Karner, P.J. Brucat, S.H. Yang, C.L. Pettiette, M.J. Craycraft, R.E. Smalley, J. Chem. Phys. 85 (1986) 1681.
[33] U. Frenzel, A. Roggenkamp, D. Kreisle, Chem. Phys. Lett. 240 (1995) 109.
[34] G. Ganteför, W. Eberhardt, H. Weidele, D. Kreisle, E. Recknagel, Phys. Rev. Lett. 77 (1996) 4524.
[35] U. Frenzel, U. Hammer, H. Westje, D. Kreisle, Z. Phys. D 40 (1997) 108.
[36] A. Amrein, R. Simpson, P. Hackett, J. Chem. Phys. 95 (1991) 1781.
[37] B.A. Collings, A.H. Amrein, D.M. Rayner, P.A. Hackett, J. Chem. Phys. 99 (1993) 4174.
[38] S.E. Kooi, A.W. Castleman Jr., J. Chem. Phys. 108 (1998) 8864.
[39] G. Schulze Icking-Konert, H. Handschuh, G. Ganteför, W. Eberhardt, Phys. Rev. Lett. 76 (1996) 1047.
[40] G. Ganteför, G. Schulze Icking-Konert, H. Handschuh, W. Eberhardt, Int. J. Mass Spectrom. Ion Processes 159 (1996) 81.
[41] R.C. Dunbar, Mass Spectrom. Rev. 11 (1992) 309.
[42] C. Walther, G. Dietrich, W. Dostal, K. Hansen, S. Krückeberg, K. Lützenkirchen, L. Schweikhard, Phys. Rev. Lett. 83 (1999) 3816.
[43] M.F. Jarrold, J.E. Bower, J. Chem. Phys. 87 (1987) 5728.
[44] S.K. Loh, D.A. Hales, L. Lian, P.B. Armentrout, J. Chem. Phys. 90 (1989) 5466.
[45] M.B. More, D. Ray, P.B. Armentrout, J. Phys. Chem. A 101 (1997) 831.
[46] M.T. Rodgers, P.B. Armentrout, J. Chem. Phys. 109 (1998) 1787.
[47] V.F. DeTuri, K.M. Ervin, J. Phys. Chem. A 103 (1999) 6911.
[48] V.A. Spasov, K.M. Ervin, J. Chem. Phys. 109 (1998) 5344.
[49] S. Roszak, K. Balasubramanian, J. Chem. Phys. 103 (1995) 1043.
[50] H. Grönbeck, W. Andreoni, Chem. Phys. Lett. 269 (1997) 385.
[51] C. Mealli, J. Am. Chem. Soc. 107 (1985) 2245.
[52] D.G. Evans, J. Organomet. Chem. 352 (1988) 397.
[53] J.P. Biberian, M.A. Van Hove, Surf. Sci. 118 (1982) 443.
[54] H. Froitzheim, M. Schulze, Surf. Sci. 211/212 (1989) 837.